

Biaxial strain tuned thermoelectric properties in monolayer PtSe₂

San-Dong Guo and Lun Zhang

Department of Physics, School of Sciences, China University of Mining and Technology, Xuzhou 221116, Jiangsu, China

Strain engineering is a very effective method to tune electronic, optical, topological and thermoelectric properties of materials. In this work, we systematically study biaxial strain dependence of electronic structures and thermoelectric properties (both electron and phonon parts) of monolayer PtSe₂ with generalized gradient approximation (GGA) plus spin-orbit coupling (SOC) for electron part and GGA for phonon part. Calculated results show that compressive or tensile strain can induce conduction band minimum (CBM) or valence band maximum (VBM) transition, which produces important effects on Seebeck coefficient. It is found that compressive or tensile strain can induce significantly enhanced n- or p-type Seebeck coefficient at the critical strain of CBM or VBM transition, which can be explained by strain-induced band convergence. Another essential strain effect is that tensile strain can produce significantly reduced lattice thermal conductivity, and the room temperature lattice thermal conductivity at the strain of -4.02% can decrease by about 60% compared to unstrained one, which is very favorable for high ZT . To estimate efficiency of thermoelectric conversion, the figure of merit ZT can be obtained by empirical scattering time τ . Calculated ZT values show that strain indeed is a very effective strategy to achieve enhanced thermoelectric properties, especially for p-type doping. Tuning thermoelectric properties with strain also can be applied to other semiconducting transition-metal dichalcogenide monolayers MX₂ (M=Zr, Hf, Mo, W and Pt; X=S, Se and Te).

PACS numbers: 72.15.Jf, 71.20.-b, 71.70.Ej, 79.10.-n

Keywords: Strain; Spin-orbit coupling; Power factor; Thermal conductivity

Email:guosd@cumt.edu.cn

I. INTRODUCTION

Thermoelectric materials have enormous potential to solve energy issues, since they can realize direct hot-electricity conversion without moving parts by using the Seebeck effect and Peltier effect. As is well known, the dimensionless figure of merit^{1,2}, $ZT = S^2\sigma T/(\kappa_e + \kappa_L)$, can measure the efficiency of thermoelectric conversion, in which S is the Seebeck coefficient, σ is electrical conductivity, T is absolute temperature, κ_e and κ_L are the electronic and lattice thermal conductivities, respectively. Bismuth-tellurium systems, lead chalcogenides and silicon-germanium alloys are the most efficient for practical application of thermoelectric devices³⁻⁵. According to the expression of ZT , high power factor ($S^2\sigma$) and low thermal conductivity ($\kappa = \kappa_e + \kappa_L$) can give rise to excellent efficiency of thermoelectric conversion, but often it is to enhance one, while adversely to affect another. Many recent advances in improving efficiency of thermoelectric conversion are focused on low-dimensional materials due to simultaneously increasing power factor and decreasing thermal conductivity⁶, such as Bi₂Te₃ nanowire, monolayer phosphorene and silicene⁷⁻⁹.

Due to the presence of intrinsic band gap, semiconducting two-dimensional (2D) transition-metal dichalcogenide monolayers have more potential application in nanoelectronics and nanophotonics in comparison with the first 2D gapless Graphene. The MoS₂ of them is hot spot of present research both experimentally and theoretically¹⁰⁻¹³, which has been applied in field effect transistors, photovoltaics and photocatalysis¹⁴⁻¹⁶. Recently, the thermoelectric properties of transition-metal dichalcogenide monolayers have attracted much

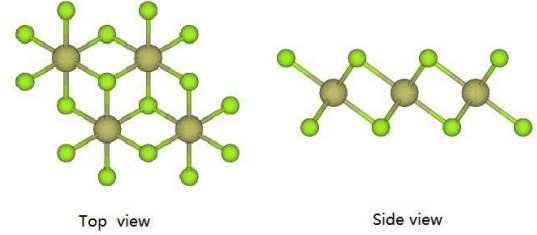


FIG. 1. (Color online) The schematic crystal structure of monolayer PtSe₂. The large balls represent Pt atoms, and small balls Se.

attention¹⁷⁻²⁴. Thermoelectric performance of MX₂ (M=Mo, W; X=S, Se) monolayers have been investigated using ab-initio method and ballistic transport model¹⁷, and at room temperature, a maximum ZT of monolayer MoS₂ is obtained as 0.5. Experimentally, a value of S as 30 mV/K has been reported for monolayer MoS₂¹⁸, which is favorable for potential thermoelectric applications. Thermoelectric response of monolayer MoSe₂ and WSe₂ also have been studied by first-principles calculations and semiclassical Boltzmann transport theory²².

Recently, we investigated spin-orbit and strain effect on power factor in monolayer MoS₂²³, and further systematically studied SOC effect on power factor in semiconducting transition-metal dichalcogenide monolayers MX₂ (M=Zr, Hf, Mo, W and Pt; X=S, Se and Te)²⁴. Among all cation groups, PtX₂ (X=S, Se and Te) show the highest Seebeck coefficient, leading to best power factor, which indicates an great potential to attain excellent thermoelectric applications. The monolayer PtSe₂ of them has been epitaxially grown by direct selenization

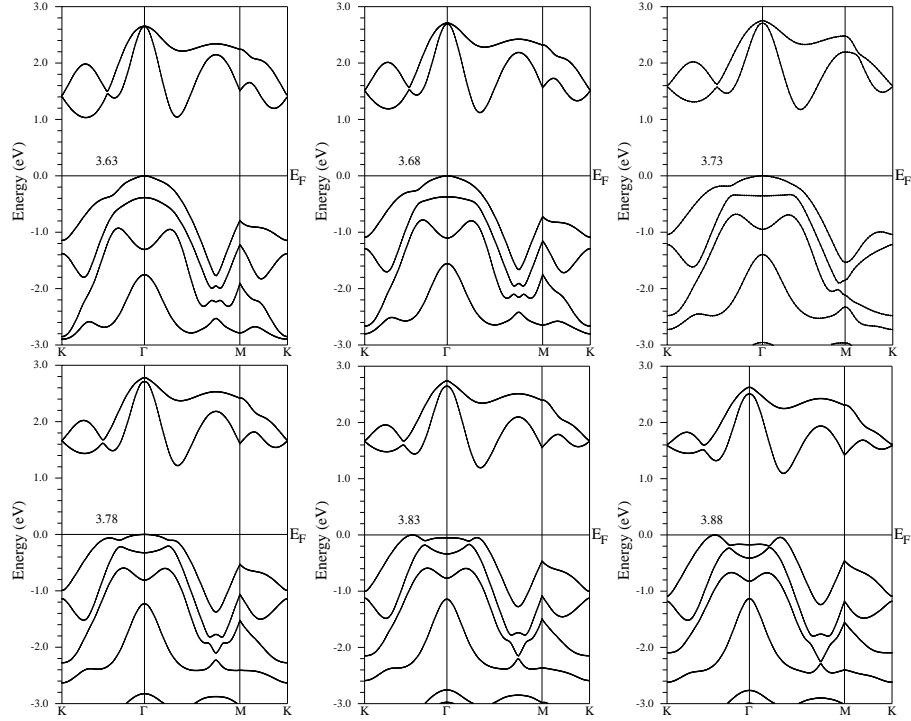


FIG. 2. The energy band structures of monolayer PtSe₂ with a changing from 3.63 Å to 3.88 Å using GGA+SOC.

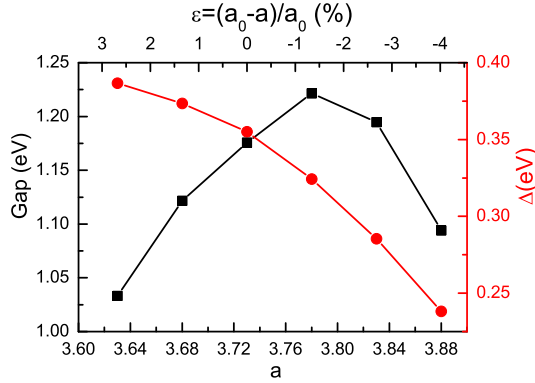


FIG. 3. (Color online) The energy band gap (Gap) and spin-orbit splitting value at Γ point (Δ) as a function of a or ε by using GGA+SOC.

of Pt with high-quality single-crystal, which has potential applications in valleytronics²⁵. Moreover, the local Rashba spin polarization and spin-layer locking in centrosymmetric monolayer PtSe₂ have been observed by using spin- and angle-resolved photoemission spectroscopy, which has potential applications in electrically tunable spintronics²⁶. The first-principles calculations show that the band gaps of monolayer PtSe₂ can be tuned over a wide range by strain engineering²⁷, but SOC is neglected, which has important effects on electronic structures of monolayer PtSe₂.

Here, the biaxial strain dependence of electronic structures and thermoelectric properties of monolayer PtSe₂

are studied. The electron part is calculated using GGA+SOC, and it is very crucial to include SOC for attaining reliable power factor^{23,24}. Calculated results show that the energy band gap first increases, and then decreases with increasing lattice constants, while the spin-orbit splitting at Γ point monotonically decreases. Compressive strain can induce CBM transition, while tensile strain can lead to VBM transition. The n- or p-type Seebeck coefficient can be significantly improved at the boundary of CBM or VBM transition, which can be understood by strain-induced accidental degeneracies. It is found that tensile strain can induce reduced lattice thermal conductivity. Finally, the ZT values are attained, which shows strain indeed can achieve enhanced thermoelectric properties.

The rest of the paper is organized as follows. In the next section, we shall describe computational details. In the third section, we shall present strain dependence of the electronic structures and thermoelectric properties of monolayer PtSe₂. Finally, we shall give our discussions and conclusion in the fourth section.

II. COMPUTATIONAL DETAIL

The strain dependence of electronic structures of monolayer PtSe₂ is performed using a full-potential linearized augmented-plane-waves method within the density functional theory (DFT)²⁸, as implemented in the WIEN2k package²⁹. We employ the popular GGA³⁰ for the exchange-correlation potential to do our elec-

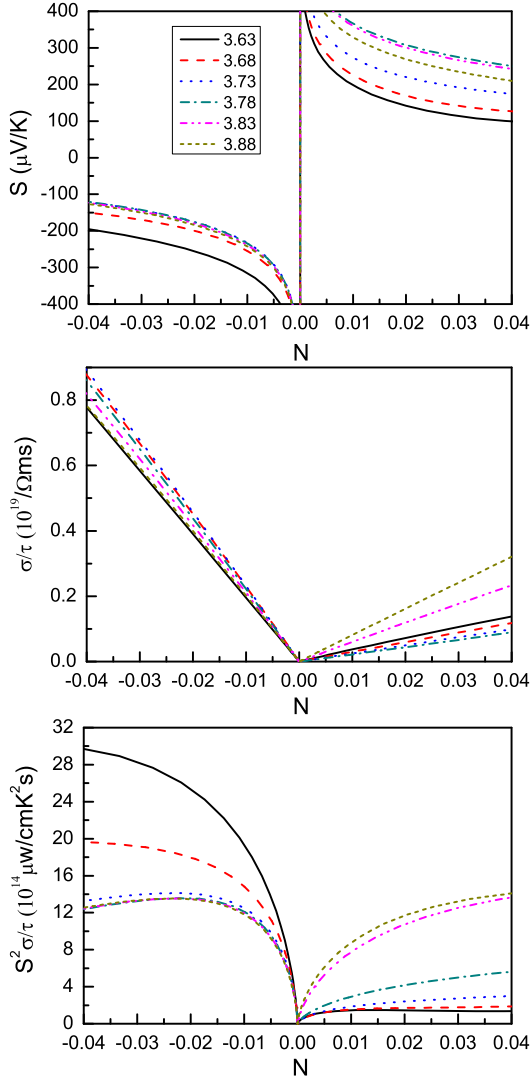


FIG. 4. (Color online) At 300 K, transport coefficients, including Seebeck coefficient S (Top), electrical conductivity with respect to scattering time σ/τ (Middle) and power factor with respect to scattering time $S^2\sigma/\tau$ (Bottom), as a function of doping level (N) with a changing from 3.63 Å to 3.88 Å using GGA+SOC. The doping level (N) means electrons (minus value) or holes (positive value) per unit cell.

tron part calculations. The internal position parameters with a force standard of 2 mRy/a.u. are optimized using GGA. The SOC was included self-consistently^{31–34} due to containing heavy elements, which produces important influences on power factor. To attain reliable results, we use 6000 k-points in the first Brillouin zone for the self-consistent calculation, make harmonic expansion up to $l_{\max} = 10$ in each of the atomic spheres, and set $R_{\text{mt}} * k_{\max} = 8$. The self-consistent calculations are considered to be converged when the integration of the absolute charge-density difference between the input and output electron density is less than $0.0001|e|$ per formula unit, where e is the electron charge. Transport calcu-

lations, such as Seebeck coefficient, electrical conductivity and electronic thermal conductivity, are performed through solving Boltzmann transport equations within the constant scattering time approximation (CSTA) as implemented in BoltzTrap³⁵, and reliable results have been obtained for several materials^{36–38}. The accurate transport coefficients need dense k-point meshes, and we use $190 \times 190 \times 1$ k-point meshes in the first Brillouin zone for the energy band calculation. The lattice thermal conductivities are calculated within the linearized phonon Boltzmann equation, which can be achieved by using Phono3py+VASP codes^{39–42}. For the third-order force constants, $3 \times 3 \times 1$ supercells are built, and reciprocal spaces of the supercells are sampled by $8 \times 8 \times 1$ meshes. To compute lattice thermal conductivities, the reciprocal spaces of the primitive cells are sampled using the $20 \times 20 \times 1$ meshes.

III. MAIN CALCULATED RESULTS AND ANALYSIS

The single-layer PtSe_2 contains three atomic sublayers with Pt layer sandwiched between two Se layers, and the schematic crystal structure is shown in Figure 1, which is different from crystal structure of MoS_2 due to different stacking of top and bottom Se or S sublayers. The unit cell of monolayer PtSe_2 contains one Pt and two Se atoms, which is constructed with the vacuum region of more than 15 Å to avoid spurious interaction between neighboring layers, and the optimized lattice constant is $a = 3.73$ Å using GGA, which is very close to the experimental value of 3.70 Å²⁵ or other theoretical value of 3.75 Å^{27,43}. The SOC has very important effects on electronic structures and thermoelectric properties, so SOC is included in all calculations of electronic part except lattice part. The energy band structures with the optimized lattice constant $a = 3.73$ Å is plotted in Figure 2, and calculated results show that PtSe_2 is an indirect gap semiconductor with a band gap of 1.18 eV. The VBM is located at Γ point, while the CBM appears between Γ and M points. The first three valence bands near the Γ point are dominated by the Se-p character states, and the fourth valence band is mostly contributed by the Pt-d states. Due to both inversion and time-reversal symmetries of PtSe_2 , all the bands are doubly degenerate.

Both theoretically and experimentally, strain influence on the electronic structures and power factor of monolayer MoS_2 has been widely studied^{23,44–46}. Here, we investigate biaxial strain effects on the electronic structures and thermoelectric properties of monolayer PtSe_2 . The $\varepsilon = (a_0 - a)/a_0$ is defined to simulate biaxial strain, and a_0 is the optimized value of 3.73 Å using GGA. $\varepsilon > 0$ means compressive strain, and $\varepsilon < 0$ implies tensile strain. Biaxial strain dependence of energy band gap and spin-orbit splitting value at Γ point in the valence bands around the Fermi level using GGA+SOC are plotted in Figure 3, and the related energy band structures

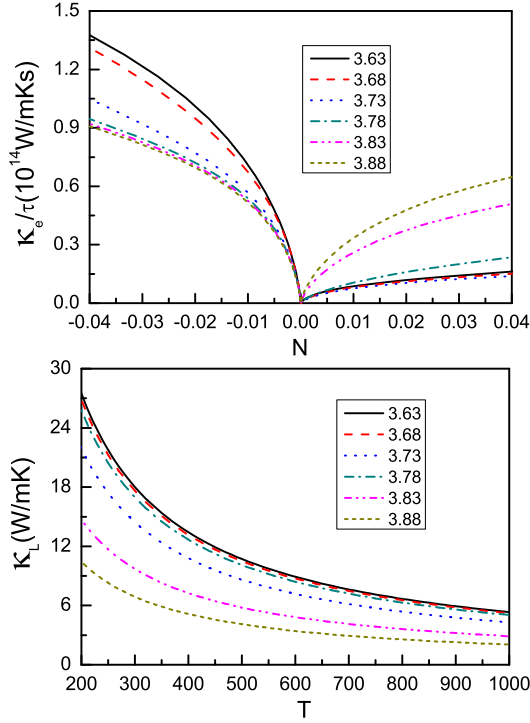


FIG. 5. (Color online) The electronic thermal conductivity with respect to scattering time κ_e/τ as a function of doping level and lattice thermal conductivity κ_L as a function of temperature with a changing from 3.63 Å to 3.88 Å.

with six considered a values are also shown in Figure 2. As the a increases, the energy band gap firstly increases, and then decreases, which is similar to strain dependence of monolayer MoS_2 ²³. The compressive strain leads to the transition of CBM from one point of Γ -M line to one point of K- Γ line, while the VBM changes from Γ point to one point of K- Γ line by applied tensile strain. The corresponding strain of CBM or VBM transition is very small, which is about 2.68%. These strain effects on electronic structures produce very important influences on power factor of monolayer PtSe_2 . As a increases, the spin-orbit splitting at Γ point monotonically decreases, and the change is about 0.15 eV with a varying from 3.63 Å to 3.88 Å. The spin-orbit splitting trend of monolayer PtSe_2 is opposite to one of MoS_2 with increasing a , and the spin-orbit splitting has stronger dependence on strain than one of MoS_2 ²³.

We perform transport coefficients calculations, such as Seebeck coefficient S and electrical conductivity with respect to scattering time σ/τ , based on CSTA Boltzmann theory. The rigid band approach is employed, which is effective for low doping level^{47–49}. The doping effects on the transport coefficients are simulated by changing the position of Fermi level. As the Fermi level moves into conduction bands, the n-type doping is achieved with negative doping levels, giving the negative Seebeck coefficient. The positive doping levels, giving the positive Seebeck coefficient, mean p-type doping, which can be

realized by shifting the Fermi level into valence bands. The biaxial strain dependence of S , σ/τ and $S^2\sigma/\tau$ using GGA+SOC at room temperature are plotted in Figure 4. The energy band structures of PtSe_2 is sensitively dependent on strain, which leads to complex strain dependence of transport coefficients. In n-type doping, compressive strain induces larger Seebeck coefficient (absolute values), while tensile strain has little effects on Seebeck coefficient. In p-type doping, the Seebeck coefficient firstly increases, and then decreases with increasing a . As a increases, the σ/τ firstly increases, and then decreases for n-type, while the opposite trend is observed for p-type. Considering the comprehensive strain effects on S and σ/τ , compressive strain can significantly enhance the n-type power factor, while tensile strain can greatly improve the p-type power factor. The similar strain effects on power factor also can be found in monolayer MoS_2 ²³.

Strain-enhanced power factor can be explained by strain-driven accidental degeneracies, namely bands converge. In considered n-type doping range, the largest S can be attained with $a=3.63$ Å among considered a due to the near degeneracy between conduction band extremum along K- Γ and one along Γ -M, leading to largest power factor. For p-type, S reaches the peak with $a=3.78$ Å, because the energy levels of one point along K- Γ line and Γ point are more adjacent. However, the lowest σ/τ is attained with $a=3.78$ Å due to more localized first valence band. The largest p-type power factor can be attained with $a=3.88$ Å due to the largest σ/τ and relatively large S . When strain is applied, the CBM or VBM transition is induced, and the corresponding critical a can produce the larger S in the considered a and doping range, which is beneficial to power factor. Calculated results show that strain-enhanced n-type power factor by using compressive strain is larger than p-type one by applied tensile strain.

Another key parameter of thermoelectric materials is thermal conductivity, including electronic and lattice thermal conductivities. The strain dependence of electronic thermal conductivity with respect to scattering time κ_e/τ (300 K) as a function of doping level and lattice thermal conductivity as a function of temperature are plotted in Figure 5. The $S^2\sigma/\tau$ has similar strain dependence with power factor. We assume that the lattice thermal conductivity is independent of doping level, and it typically goes as $1/T$ at high temperature. It is found that tensile strain can induce lower lattice thermal conductivity, which is very beneficial to the efficiency of thermoelectric conversion. The room temperature lattice thermal conductivity ($6.88 \text{ Wm}^{-1}\text{K}^{-1}$) with $a=3.88$ Å is about 60% smaller than that ($16.97 \text{ Wm}^{-1}\text{K}^{-1}$) with optimized lattice constant $a=3.73$ Å.

Finally, the $S^2\sigma/\tau$ and κ_e/τ as a function of temperature with the doping concentration of $2.012 \times 10^{13} \text{ cm}^{-2}$ for both n- and p-type are shown in Figure 6. In the considered temperature range, the strain dependence of both $S^2\sigma/\tau$ and κ_e/τ is consistent with one at 300 K. The n-type power factor with $a=3.63$ Å and p-type one

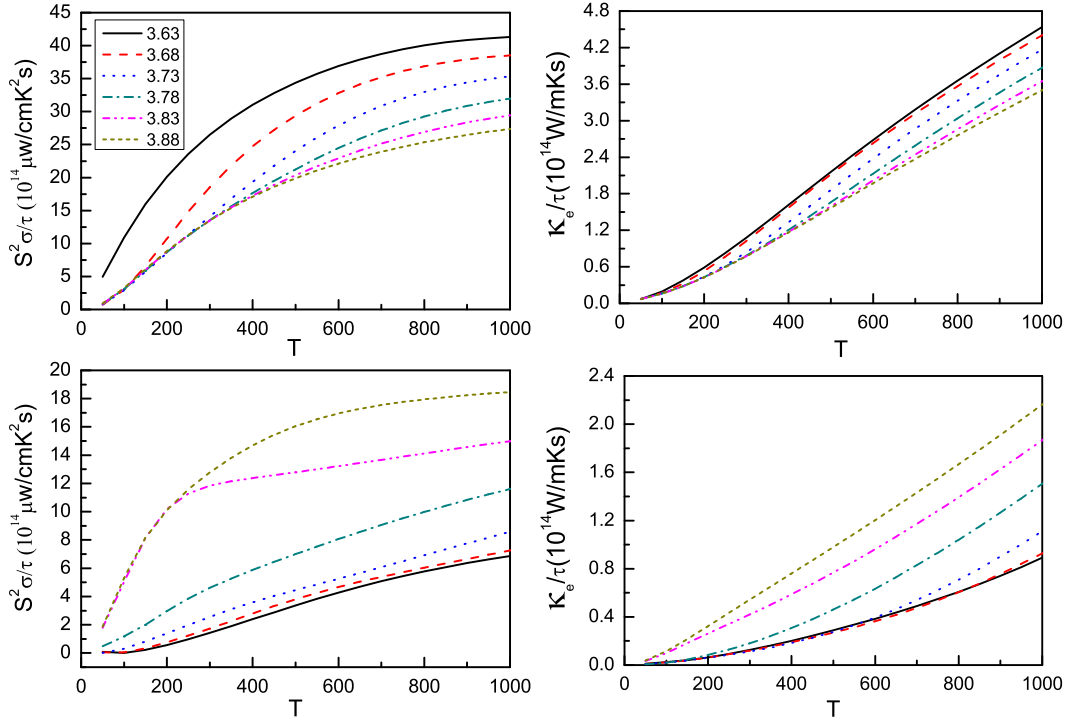


FIG. 6. (Color online) For both n-type (Top) and p-type (Bottom), the power factor with respect to scattering time $S^2\sigma/\tau$ and electronic thermal conductivity with respect to scattering time κ_e/τ as a function of temperature with a changing from 3.63 Å to 3.88 Å using GGA+SOC, and the doping concentration is $2.012 \times 10^{13} \text{ cm}^{-2}$ (about 0.025 electrons or holes per unit cell).

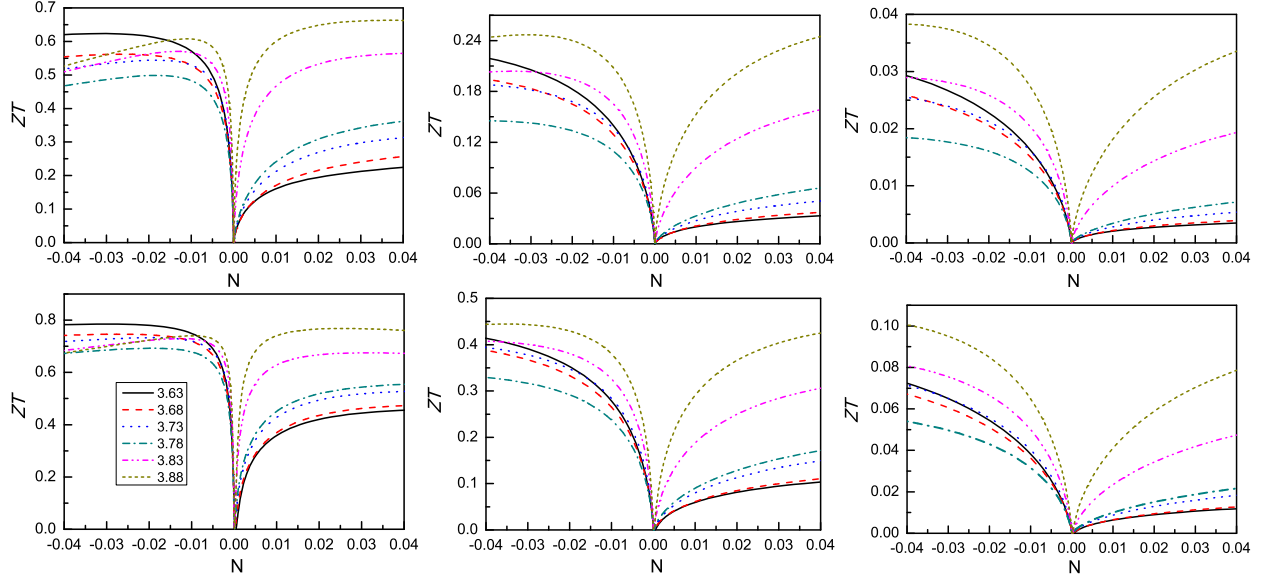


FIG. 7. (Color online) At 600 K (Top) and 900 K (Bottom), the ZT as a function of doping level with a changing from 3.63 Å to 3.88 Å, and the scattering time τ is 1×10^{-13} s (Left), 1×10^{-14} s (Middle) and 1×10^{-15} s (Right).

with $a=3.88$ Å are the largest among the considered a . To attain figure of merit ZT , the scattering time τ is unknown. Calculating scattering time τ is challenging from the first-principle calculations due to the complexity of various carrier scattering mechanisms. To attain possible ZT values, the scattering time τ is assumed to be $1 \times$

10^{-13} s, 1×10^{-14} s and 1×10^{-15} s. In Ref.²¹, the scattering time of monolayer MoS₂ is fitted as $2.29 \sim 5.17 \times 10^{-14}$ s to calculate ZT . For WSe₂, the scattering time is found to be 1.6×10^{-13} or 1.4×10^{-15} s²². Therefore, our assumed scattering time should be reasonable. At 600 K and 900 K, the ZT as a function of doping level

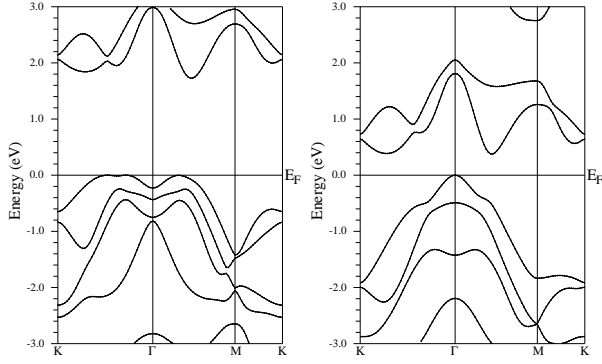


FIG. 8. The energy band structures of monolayer PtS₂ (Left) and PtTe₂ (Right) with unstrained lattice constants using GGA+SOC.

with a changing from 3.63 Å to 3.88 Å are plotted in Figure 7. The similar strain dependence between 600 K and 900 K is observed except for relative sizes of ZT . It is found that the ZT decreases with decreasing τ , which is because the larger τ produces larger power factor. In p-type doping, tensile strain can observably improve the ZT for all three τ . For n-type, tensile strain can also enhance the ZT with $\tau=1 \times 10^{-14}$ s and $\tau=1 \times 10^{-15}$ s. However, compressive strain can slightly improve ZT with $\tau=1 \times 10^{-13}$ s. The peak ZT is about 0.65, 0.25 and 0.04 with decreasing τ at 600 K, and 0.80, 0.45 and 0.1 at 900 K. Calculated results show that tensile strain may be a effective method to attain higher ZT , which can achieve higher thermoelectric conversion efficiency.

IV. DISCUSSIONS AND CONCLUSION

The semiconducting transition-metal dichalcogenide monolayers may be potential thermoelectric materials. However, huge works focused on thermoelectric properties of monolayer MoS₂. In Ref.²⁴, we systematically investigated electronic transport properties of semiconducting transition-metal dichalcogenide monolayers MX₂ (M=Zr, Hf, Mo, W and Pt; X=S, Se and Te), including SOC. Among all cation groups, Pt cation group exhibits best power factor due to the highest Seebeck coefficient, assuming scattering time to be fixed. Here, recent synthetic PtSe₂ is investigated, whose room temperature lattice thermal conductivity (16.97 Wm⁻¹K⁻¹) is lower than one (26.2 Wm⁻¹K⁻¹¹¹⁹) of monolayer MoS₂ with the similar calculation method. So, monolayer PtSe₂ may possess better thermoelectric properties than monolayer MoS₂. The high lattice thermal conductivity is a major disadvantage to obtain higher ZT . However, the lattice thermal conductivity can be reduced by phonon engineering, such as isotope doping⁵⁰, nanoporous structure⁵¹ or strain⁵². The typical example is graphene, whose lattice thermal conductivity can be reduced largely by phonon engineering, producing a very high ZT of 3⁵³. The pressure-reduced lattice thermal conductivity also

can be found in Mg₂Sn⁵². Here, tensile strain can induce remarkably reduced lattice thermal conductivity, from 16.97 Wm⁻¹K⁻¹ to 6.88 Wm⁻¹K⁻¹ at 300 K with a changing from 3.73 Å to $a=3.88$ Å, and the corresponding ε is about -4.02%, which should be easily achieved in experiment by piezoelectric stretching and exploiting the thermal expansion mismatch^{54,55}.

The electronic structures of semiconducting transition-metal dichalcogenide monolayers is quite sensitive to strain, which provides a strategy to tune their thermoelectric properties by band engineering. Strain or pressure is a conventional way to induce novel phenomenon, such as pressure-induced high-T_c superconductivity^{56,57} and strain-induced topological insulator⁵⁸. The symmetry-driven degeneracy, low-dimensional electronic structures and accidental degeneracies are three usual mechanisms to induce high Seebeck coefficient suitable for high power factor. Here, strain-induced accidental degeneracies, namely band convergence, can be used to explain strain-enhanced Seebeck coefficient. For optimized lattice constants $a=3.73$ Å, monolayer PtSe₂ has some valence band extrema (VBE) and conduction band extrema (CBE) around the Fermi level, which provides a platform to achieve band convergence by strain. When compressive strain gradually increases, the CBE along K-Γ and Γ-M approach each other, and the energy difference changes from 0.140 eV to 0.009 eV with a being 3.73 Å to 3.63 Å. The conduction band convergence produces large n-type Seebeck coefficient, giving rise to high n-type power factor. When tensile strain gradually increases, the VBE along K-Γ and VBM are more close, and the energy difference varies from 0.184 eV to 0.062 eV with a changing from 3.73 Å to 3.78 Å. The valence band convergence induces large p-type Seebeck coefficient. As the a continues to increase, the extrema at Γ point disappears, and another extrema along Γ-M appears, which induces significantly enhanced p-type electrical conductivity. The largest p-type power factor achieves at $a=3.88$ Å. Calculated results show that the large Seebeck coefficient can be induced by both compressive and tensile strain at the critical strain of CBM or VBM transition. Similar pressure or strain induced band convergence, leading to large Seebeck coefficient, also can be found in Mg₂Sn⁵² at the critical pressure of energy band gap or monolayer MoS₂ at the critical strain of direct-indirect gap transition²³. The n-type doping related results indicates that a large power factor will not certainly produce a high ZT , while a moderate power factor combined with a suitable thermal conductivity may eventually lead to a high ZT .

In fact, band convergence can be observed in unstrained PtS₂ and PtTe₂, and the energy band structures of monolayer PtS₂ and PtTe₂ with unstrained lattice constants 3.57 Å and 4.02 Å using GGA+SOC are plotted in Figure 8. For PtS₂, valence band convergence can be observed, and the similar results for PtSe₂ can be achieved by tensile strain. For PtTe₂, conduction band convergence can be seen, which can be attained for

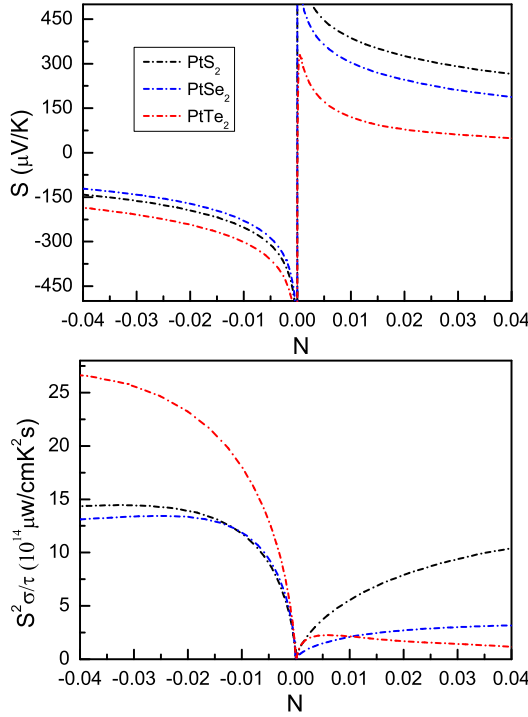


FIG. 9. (Color online) At 300 K, transport coefficients of PtX_2 ($X=\text{S}$, Se and Te) with unstrained lattice constants, including Seebeck coefficient S (Top) and power factor with respect to scattering time $S^2\sigma/\tau$ (Bottom), as a function of doping level (N) using GGA+SOC.

PtSe_2 by compressive strain. Band convergence is favorable for Seebeck coefficient, leading to high power factor. To clearly illustrate these results, the room temperature transport coefficients of PtX_2 ($X=\text{S}$, Se and Te) with unstrained lattice constants, including Seebeck coefficient S

and power factor with respect to scattering time $S^2\sigma/\tau$, as a function of doping level using GGA+SOC are shown in Figure 9. It is very clear to see that PtS_2 (PtTe_2) has the largest p-type (n-type) Seebeck coefficient, which is consistent with corresponding band convergence. It is resultant that PtS_2 (PtTe_2) has the highest p-type (n-type) power factor.

In summary, we systematically study strain dependence of thermoelectric properties of monolayer PtSe_2 , including both electron and phonon transport, using GGA+SOC, based mainly on the reliable first-principle calculations. It is found that both compressive and tensile strain can induce improved Seebeck coefficient at the critical strain of CBM or VBM transition, which is favorable for power factor. Calculated results also show that tensile strain can lead to significantly reduced lattice thermal conductivity, which is beneficial to ZT . By using hypothetical scattering time τ , ZT can be obtained, which shows that strain indeed can induce enhanced efficiency of thermoelectric conversion due to improved ZT value. So, strain is a very effective method to achieve enhanced thermoelectric properties for monolayer PtSe_2 , which provides great opportunities for efficient thermoelectricity. The strategy of strain-tuned thermoelectric properties also can be used in other semiconducting transition-metal dichalcogenide monolayers, like PtS_2 and PtTe_2 with high power factor.

ACKNOWLEDGMENTS

This work is supported by the National Natural Science Foundation of China (Grant No. 11404391). We are grateful to the Advanced Analysis and Computation Center of CUMT for the award of CPU hours to accomplish this work.

- ¹ Y. Pei, X. Shi, A. LaLonde, H. Wang, L. Chen and G. J. Snyder, *Nature* **473**, 66 (2011).
- ² A. D. LaLonde, Y. Pei, H. Wang and G. J. Snyder, *Mater. Today* **14**, 526 (2011).
- ³ W. S. Liu, Q. Y. Zhang, Y. C. Lan, S. Chen, X. Yan, Q. Zhang, H. Wang, D. Z. Wang, G. Chen and Z. F. Ren, *Adv. Energy Mater.* **1**, 577 (2011).
- ⁴ Y. Z. Pei, X. Y. Shi, A. Lalonde et al. *Nature* **473**, 66 (2011).
- ⁵ M. Zebarjadi, et al. *Nano Lett.* **11**, 2225 (2011).
- ⁶ M. S. Dresselhaus et al. *Adv. Mater.* **19**, 1043 (2007).
- ⁷ G. Zhang, B. Kirk, L. A. Jauregui, H. Yang, X. Xu, Y. P. Chen and Y. Wu, *Nano Lett.* **12**, 56 (2012).
- ⁸ R. Fei, A. Faghaninia, R. Soklaski, J. A. Yan, C. Lo and L. Yang, *Nano Lett.* **14**, 6393 (2014).
- ⁹ K. Yang, S. Cahangirov, A. Cantarero, A. Rubio and R. D'Agosta, *Phys. Rev. B* **89**, 125403 (2014).
- ¹⁰ K. F. Mak, C. Lee, J. Hone, J. Shan, and T. F. Heinz, *Phys. Rev. Lett.* **105**, 136805 (2010).
- ¹¹ A. Splendiani, L. Sun, Y. Zhang, T. Li, J. Kim, C. Y. Chim, G. Galli and F. Wang, *Nano Lett.* **10**, 1271 (2010).
- ¹² S. Lebegue and O. Eriksson, *Phys. Rev. B* **79**, 115409 (2009).
- ¹³ C. Ataca, H. Sahin, E. Akturk and S. Ciraci, *J. Phys. Chem. C* **115**, 3934 (2011).
- ¹⁴ S. Ghatak, A. N. Pal and A. Ghosh, *Acs Nano* **5**, 7707 (2011).
- ¹⁵ B. Radisavljevic, A. Radenovic, J. Brivio, V. Giacometti and A. Kis, *Nature Nanotechnology* **6**, 147 (2011).
- ¹⁶ X. Zong et al. *J. Am. Chem. Soc.* **130**, 7176 (2008).
- ¹⁷ W. Huang, H. X. Da and G. C. Liang, *J. Appl. Phys.* **113**, 104304 (2013).
- ¹⁸ J. Wu et al. *Nano Lett.* **14**, 2730 (2014).
- ¹⁹ X. Wei et al. *Appl. Phys. Lett.* **105**, 103902 (2014).
- ²⁰ W. Li, J. Carrete and N. Mingo, *Appl. Phys. Lett.* **103**, 253103 (2013).
- ²¹ Z. Jin et al. *Sci. Rep.* **5**, 18342 (2015).
- ²² S. Kumar and U. Schwingenschlöggl, *Chem. Mater.* **27**, 1278 (2015).
- ²³ S. D. Guo, *Comp. Mater. Sci.* **123**, 8 (2016).

- ²⁴ S. D. Guo and J. L. Wang, *Semicond. Sci. Tech.* in press.
- ²⁵ Y. L. Wang et al. *Nano Lett.* **15**, 4013 (2015).
- ²⁶ W. Yao et al. arXiv:1603.02140.
- ²⁷ P. F. Li, L. Li and X. C. Zeng, *J. Mater. Chem. C*, **4**, 3106 (2016).
- ²⁸ P. Hohenberg and W. Kohn, *Phys. Rev.* **136**, B864 (1964); W. Kohn and L. J. Sham, *Phys. Rev.* **140**, A1133 (1965).
- ²⁹ P. Blaha, K. Schwarz, G. K. H. Madsen, D. Kvasnicka and J. Luitz, WIEN2k, an Augmented Plane Wave + Local Orbitals Program for Calculating Crystal Properties (Karlheinz Schwarz Technische Universität Wien, Austria) 2001, ISBN 3-9501031-1-2
- ³⁰ J. P. Perdew, K. Burke and M. Ernzerhof, *Phys. Rev. Lett.* **77**, 3865 (1996).
- ³¹ A. H. MacDonald, W. E. Pickett and D. D. Koelling, *J. Phys. C* **13**, 2675 (1980).
- ³² D. J. Singh and L. Nordstrom, *Plane Waves, Pseudopotentials and the LAPW Method*, 2nd Edition (Springer, New York, 2006).
- ³³ J. Kunes, P. Novak, R. Schmid, P. Blaha and K. Schwarz, *Phys. Rev. B* **64**, 153102 (2001).
- ³⁴ D. D. Koelling, B. N. Harmon, *J. Phys. C: Solid State Phys.* **10**, 3107 (1977).
- ³⁵ G. K. H. Madsen and D. J. Singh, *Comput. Phys. Commun.* **175**, 67 (2006).
- ³⁶ B. L. Huang and M. Kaviani, *Phys. Rev. B* **77**, 125209 (2008).
- ³⁷ L. Q. Xu, Y. P. Zheng and J. C. Zheng, *Phys. Rev. B* **82**, 195102 (2010).
- ³⁸ J. J. Pulikkotil, D. J. Singh, S. Auluck, M. Saravanan, D. K. Misra, A. Dhar and R. C. Budhani, *Phys. Rev. B* **86**, 155204 (2012).
- ³⁹ G. Kresse, *J. Non-Cryst. Solids* **193**, 222 (1995).
- ⁴⁰ G. Kresse and J. Furthmüller, *Comput. Mater. Sci.* **6**, **15** (1996).
- ⁴¹ G. Kresse and D. Joubert, *Phys. Rev. B* **59**, 1758 (1999).
- ⁴² A. Togo, L. Chaput and I. Tanaka, *Phys. Rev. B* **91**, 094306 (2015).
- ⁴³ H. L. Zhuang and R. G. Hennig, *J. Phys. Chem. C* **117**, 20440 (2013).
- ⁴⁴ K. L. He, C. Poole, K. F. Mak and J. Shan, *Nano Lett.* **13**, 2931 (2013).
- ⁴⁵ H. L. Shi, H. Pan, Y. W. Zhang and B. I. Yakobson, *Phys. Rev. B* **87**, 155304 (2013).
- ⁴⁶ T. Cheiwchanchamnangij, W. R. L. Lambrecht, Y. Song and H. Dery, *Phys. Rev. B* **88**, 155404 (2013).
- ⁴⁷ T. J. Scheidemantel, C. Ambrosch-Draxl, T. Thonhauser, J. V. Badding and J. O. Sofo, *Phys. Rev. B* **68**, 125210 (2003).
- ⁴⁸ G. K. H. Madsen, *J. Am. Chem. Soc.* **128**, 12140 (2006).
- ⁴⁹ X. Gao, K. Uehara, D. Klug, S. Patchkovskii, J. Tse and T. Tritt, *Phys. Rev. B* **72**, 125202 (2005).
- ⁵⁰ N. Yang, Z. Gang and B. Li, *Nano Lett.* **8**, 276 (2007).
- ⁵¹ J. Y. Tang et al. *Nano Lett.* **10**, 4279 (2010).
- ⁵² S. D. Guo and J. L. Wang, *RSC Adv.* **6**, 31272 (2016).
- ⁵³ P. H. Chang, M. S. Bahrany, N. Nagaosa and B. K. Nikolic, *Nano Lett.* **14**, 3779 (2014).
- ⁵⁴ Y. Y. Hui et al. *ACS Nano* **7**, 7126 (2013).
- ⁵⁵ G. Plechinger et al. *2D Mater.* **2**, 015006 (2015).
- ⁵⁶ D. F. Duan, Y. X. Liu, F. B. Tian, D. Li, X. L. Huang, Z. L. Zhao, H. Y. Yu, B. B. Liu, W. J. Tian and T. Cui, *Sci. Rep.* **4**, 6968 (2014).
- ⁵⁷ A. P. Drozdov, M. I. Erements, I. A. Troyan, V. Ksenofontov and S. I. Shylin, *Nature* **525**, 73 (2015).
- ⁵⁸ W. L. Liu, X. Y. Peng, C. Tang, L. Z. Sun, K. W. Zhang, and J. X. Zhong, *Phys. Rev. B* **84**, 245105 (2011).